A SIMPLE AND ROBUST DESTRIPING ALGORITHM FOR IMAGING SPECTROMETERS: APPLICATION TO MODIS DATA

Marouan Bouali[1,2]
[1]CNES, Toulouse, France
[2]INRIA , Le Chesnay, France
marouan.bouali@inria.fr

ABSTRACT

Images provided by several imaging spectrometers are often contaminated with stripes. This artifact compromises the visual quality and radiometric integrity of measured data. Although a large number of destriping algorithms have been recently suggested, most of them provide results that display residual stripes if not strong distortion from the original signal. To overcome this issue, we introduce a robust methodology using a gradient-based iterative destriping algorithm (GBIDA). Statistical assumptions used in previous methods such as histogram matching are replaced with a more realistic geometrical consideration on the images spatial gradient. An iterative scheme is then used in order to isolate the striping effect from the original image prior to processing. Application of this method on MODIS level 1B images heavily affected with detector-to-detector stripes, mirror-side stripes and random stripes displays excellent qualitative and quantitative results; the visual quality of the images is greatly improved without introduction of any blurring effect. This new destriping technique is easy to implement and can be applied to denoise data derived from many imaging spectrometers.

INTRODUCTION

The Moderate Resolution Imaging Spectrometer (MODIS) was successfully launched aboard the Earth Observing System (EOS) Terra and Aqua. MODIS enables a monitoring of the entire earth's surface in 36 spectral bands ranging from the visible to the long-wave infrared at spatial resolutions of 1km, 500 meters and 250 meters. Since 1999, MODIS has been constantly providing a wide range of remote sensing products that helped scientists dig further in the understanding of earth climate and the dynamic interactions involved between land, ocean and atmosphere. Currently, an increasing community of scientists is actively involved in the improvement of remote sensing data quality. For instance, a common artifact of imaging spectrometers is the well-known striping effect, clearly visible in most of MODIS products generated using emissive bands. This noise is directly related to MODIS cross-track, double-sided, continously rotating scan mirror that deflects the measured energy to photon detectors. Gumley (Gumley, 2002) identified three types of stripes in MODIS data. Detector-to-detector stripes are induced by a poor calibration of the relative gain and offset of each detector. These periodic stripes can be observed in the entire acquired image and are due to the slight deviation that exists between the input/output trunsfer function of different detectors. Plus, these deviations are not constant over time because they depend on the photomultipliers exposure history (Wegener, 1990). Mirror side stripes also known as mirror banding are due to a quasi constant offset between forward and reverse scans and are dependent on the signal intensity level. It is often visible over bright targets with reflectance values high enough to bring the sensor close to its saturation mode. A typical case of mirror banding can be seen in homogeneous oceanographic images affected with sun glint or strong atmospheric effects. Because mirror side stripe is related to the radiance level, it is not necesserely present in the whole image and is correlated to the scan angle. Noisy stripes, are random and only affect specific thermal bands. They appear as bright and dark stripes with a given lenght over a scan line. In all cases, the presence of stripes cannot only be attributed to the imperfect relative calibration of the sensor detectors because other factors such as source spectral distribution and polarization, or random noise in the internal calibration system can intervene (Simpson and Yhann 1994, Algazi and Ford 1981). The algorithms proposed in the destriping litterature can be classified in different categories. The first class of destriping methods relies on digital filtering (Crippen 1989, Srinivasan et al. 1988, Pan and Chang 1992, Simpson et al. 1995, Simpson et al. 1998, Chen et al. 2003), and takes advantage of stripes periodicity to remove its spatial frequency. Although easy to implement, and sensor independent, these techniques introduce a blurring effect equivalent to a loss of radiometric accuracy. The second category focuses on the

statistical properties of data measured by each individual detector. The moment matching technique presented in (Horn and Woodham 1979), removes stripes by assuming that the mean and standard deviation of the data measured by each detector are identical. Horn and Woodham suggested an improvement based on the histogram matching technique. The image is considered as a signal with a given empirical cumulative distribution function (ECDF). The data acquired by each detector is subsequently modified in order to fit an imposed reference ECDF. These statistics-based methods display good results, but their performance is limited by a criterion of homogeneity due to the strong assumption of sub-detectors viewing the same scene. Over the years, many improved algorithms have been suggested, combining basic destriping methods with advanced image processing techniques. In (Chang et al. 2007) the authors combined moment matching with wavelet analysis. Facet filtering was used in (Rakwatin et al. 2007) and combined with histogram matching to reduce the effects of random stripes in MODIS images. In (Corsini et al. 2000), the authors developped a destriping algorithm for the Modular Optoelectronic Scanner B-data (MOS-B). Assuming that stripes are constant with time, a data set of quasi homogeneous images of sea targets acquired by MOS-B was used to determine the equalisation curves for each detector prior to stripe removal. The destriping methodology proposed in (Antonelli et al. 2004) takes advantage of another artifact present in MODIS images, the bow-tie effect. When the scanning angle is higher than ±25°, two consecutive detectors happen to observe the same instantaneous field of view (IFOV), and thus redundent information from scan-to-scan overlaps can be exploited to establish an equalisation curve and provide an additional calibration of detectors. This destriping methodology was extensively investigated in (Biscelie et al. 2009). Recently, variational approaches has become a popular alternative for image denoising and image restoration applications. In (Shen and Zhang, 2009), the authors used a maximum a priori (MAP)-based algorithm to remove striping from MODIS data, and obtained promising results. However, the regularisation model used (Hubert-Markov) does not take advantage of the striping effect unidirectional signature.

In this paper, we introduce an effective destriping methodology able to isolate the striping effect from the original signal using an intuitive divide & conquer approach. We show that our algorithm is equivalent to an optimisation problem and we provide its variational formulation. Our method is tested on MODIS imagery and compared qualitatively and quantitatively to other destriping techniques. The next section of this paper describes the mathematical formulation of the destriping algorithm and is followed by illustrated experimental results, conclusion and futur work.

DESTRIPING ALGORITHM

Integration of 2D gradient fields is a well known issue in many computer vision and computers graphics applications such as photometric stereo and shape from shading recovery. Given a gradient field, the idea is to recover a surface whose gradients approximates the input gradient field. This ill-posed problem can be solved using multigrid methods, fast marching methods, or fast Poisson solvers. In (Frankot and Chellapa, 1988), the authors suggested to minimise a least square cost energy functional, and solved the Poisson equation by shifting in fourier space. Let us denote by **I** the original striped image defined in Ω, a bunded domain of $\Re^2$, and consider the following energy functional:

$$E_x(u) = \int_{\Omega} \left\| \frac{\partial (u - I)}{\partial x} \right\|^2 + \left\| \frac{\partial u}{\partial y} \right\|^2 dxdy \tag{1}$$

The solution $\boldsymbol{u}$ that minimises the previous equation satistifies the Euler-Lagrange equation:

$$0 - 2\frac{\partial}{\partial x}\left(\frac{\partial u}{\partial x} - \frac{\partial I}{\partial x}\right) - 2\frac{\partial}{\partial y}\left(\frac{\partial u}{\partial y}\right) = 0 \tag{2}$$

The previous equation can be rearranged to:

$$\nabla^2 u = \frac{\partial^2 I}{\partial^2 x} \tag{3}$$

Let us denote by $\mathbf{f_x}$ (resp. $\mathbf{f_y}$) the horizontal (resp. vertical) frequency variables and recall the following differenciation properties of the fourier transform:

$$\begin{aligned} F\left(\partial u / \partial x\right) &= j.f_x F\left(u\right) & \qquad F\left(\partial u / \partial y\right) &= j.f_y F\left(u\right) \\ F\left(\partial^2 u / \partial^2 x\right) &= f_x{}^2 F\left(u\right) & \qquad F\left(\partial^2 u / \partial^2 y\right) &= f_y{}^2 F\left(u\right) \end{aligned} \tag{4}$$

The fourier transform of equation (3) is then given by:

$$f_x{}^2 U_F + f_y{}^2 U_F = f_x{}^2 I_F \tag{5}$$

where $\mathbf{U_F}$ and $\mathbf{I_F}$ are the fourier transforms of the estimated solution $\boldsymbol{u}$ and the original striped image $\mathbf{I}$. The minimization of the functional (1) is given in fourier space by:

$$U_{xF} = \frac{f_x{}^2}{f_x{}^2 + f_y{}^2} I_F = R_x I_F \tag{6}$$

Using the same methodology, the minimization of the following functional:

$$E_y(u) = \int_\Omega \left\| \frac{\partial u}{\partial x} \right\|^2 + \left\| \frac{\partial (u - I)}{\partial y} \right\|^2 dxdy \tag{7}$$

is given in fourier space by:

$$U_{yF} = \frac{f_y{}^2}{f_x{}^2 + f_y{}^2} I_F = R_y I_F \tag{8}$$

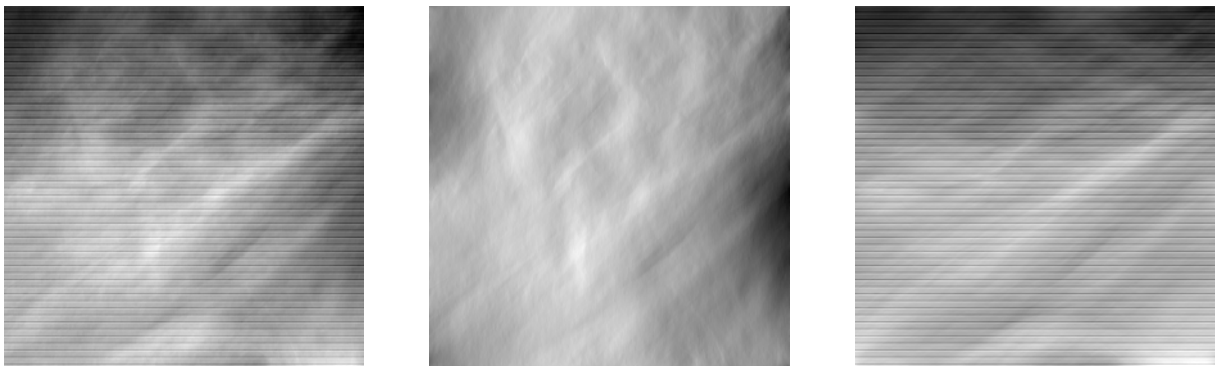

(a) (b) (c)

Figure 1. (a) Original striped image from MODIS Aqua band 27, acquired on 10th november 2009, western California (b) Solution of the minimization of functional (1) (c) Solution of the minimization of functional (7).

A visual inspection of the images associated with equations (6) and (8) (displayed in fig.1) shows that (1) the image resulting from the minimisation of the functional (1) is not affected with stripes (2) the image resulting from the minimisation of (7) is still striped but displays softer variations along the x-axis (3) The mathematical expression of equations (6) and (8) leads to the triviality:

$$I_F = U_{xF} + U_{yF} = \left(R_x + R_y\right) I_F \tag{9}$$

Visually, the image shown in figure 1b can be considered as a first order approximation of the destriped image. An intuitive way to improve this approximation is to adopt a simple divide & conquer strategy. Because stripes are only present in the term $\mathbf{R_y I_F}$ (figure 1c), a second iteration will consist in minimizing functionals (1) and (7) where the original image **I** is replaced by the solution of the minimization of (7) in the first iteration, i.e. , the inverse fourier transform of $\mathbf{R_y I_F}$. In the second iteration, the image can then be decomposed as:

$$I_F = \left(R_x + R_x R_y + R_y^{\,2}\right) I_F \tag{10}$$

The $\mathbf{N}^{th}$ iteration leads to an expression of the following form:

$$I_F = \left(P\left(R_x\right) + R_y^{\,N}\right) I_F \tag{11}$$

where ***P*** denotes a polynome of order **N**. The interesting point in this decomposition is that the stripping effect is isolated in the second term of the previous equation. For a number of iterations **N** high enough, this offers the possibility to apply a low-pass filter only on the term $\mathbf{R_y^N I_F}$ and thus avoid the introduction of any blurring effect. It is important to mention that the digital filter is used strictly to impose the mean values of the destriped image lines. Let us denote by H_F a suitable low-pas filter in fourier space. The destriped image is then given by:

$$I_F = \left(P\left(R_x\right) + H_F R_y^{\,N}\right) I_F \tag{12}$$

Using a reverse procedure than the one used to derive the minimisation solutions of (1) and (7) in fourier space, it can be shown that from a variational framework, our algorithm consists in miniming the following energy functional:

$$E_N(u) = \int_\Omega \sum_{\substack{i+j=N \\ j \neq N}} \frac{N!}{i!(N-i)!} \left\| \frac{\partial (u - I)}{\partial^i x \partial^j y} \right\|^2 + \left\| \frac{\partial^N (u - H_F I)}{\partial^N y} \right\|^2 dxdy \tag{13}$$

The choice of the number of iterations **N**, is an important aspect of our destriping algorithm. It can be shown that for
$\mathbf{N} \to \infty$, our algorithm is equivalent to removing the mean value of each line in the image $\boldsymbol{P}(\mathbf{R_x})\mathbf{I_F}$. In the case of MODIS data, this does not account for detectors non-linearities, and will display similar results to those provided by moment matching or histogram matching. Therefore, the destriping procedure should be stopped as soon as a satisfactory image distortion is reached, i.e. , ID ≈ 0.95 (the image distortion index is defined in the next section).

EXPERIMENTAL RESULTS

In this paper, we used MODIS Aqua and Terra level 1B data downloaded from the Level 1 and Atmosphere Archive and Distribution System (http://ladsweb.nascom.nasa.goc/). MODIS level 1B data corresponds to Top of Atmosphere calibrated radiances coded to a 16-bit scale and are in hierarchical data format-EOS format, the standard format for Terra and Aqua sensors. To illustrate the visual quality improvement, we selected two scenes acquired respectively by Aqua MODIS and Terra MODIS in western California, in November 10, 2009 and March 4, 2008. The algorithm output is illustrated on images of 512×512 pixels extracted from emissive band 27 (6.535-6.895 µm) and band 33 (13.185-13.485 µm), at 1 km resolution. These bands have been choosen for our study because they are affected by all types of stripes including radom stripes. This allows us to assess the robustness of our destriping procedure. Figures 2 and 4 show the visual quality improvement provided by low-pass filtering, histogram matching and the proposed algorithm (GBIDA). Visual analysis of images shows that our approach removes effectively all types of stripes without any blurring effect. Figure 3 displays the mean cross-track profiles

before and after destriping. As expected, cross-track profiles of the original striped images display strong periodic and random variations from a line to another. These fluctuations are expected to be properly filtered according to the efficiency of the adopted destriping approach. For instance, figures 3c and 5c clearly show that the histogram matching technique only corrects for detector-to-detector stripes and mirror side stripes.

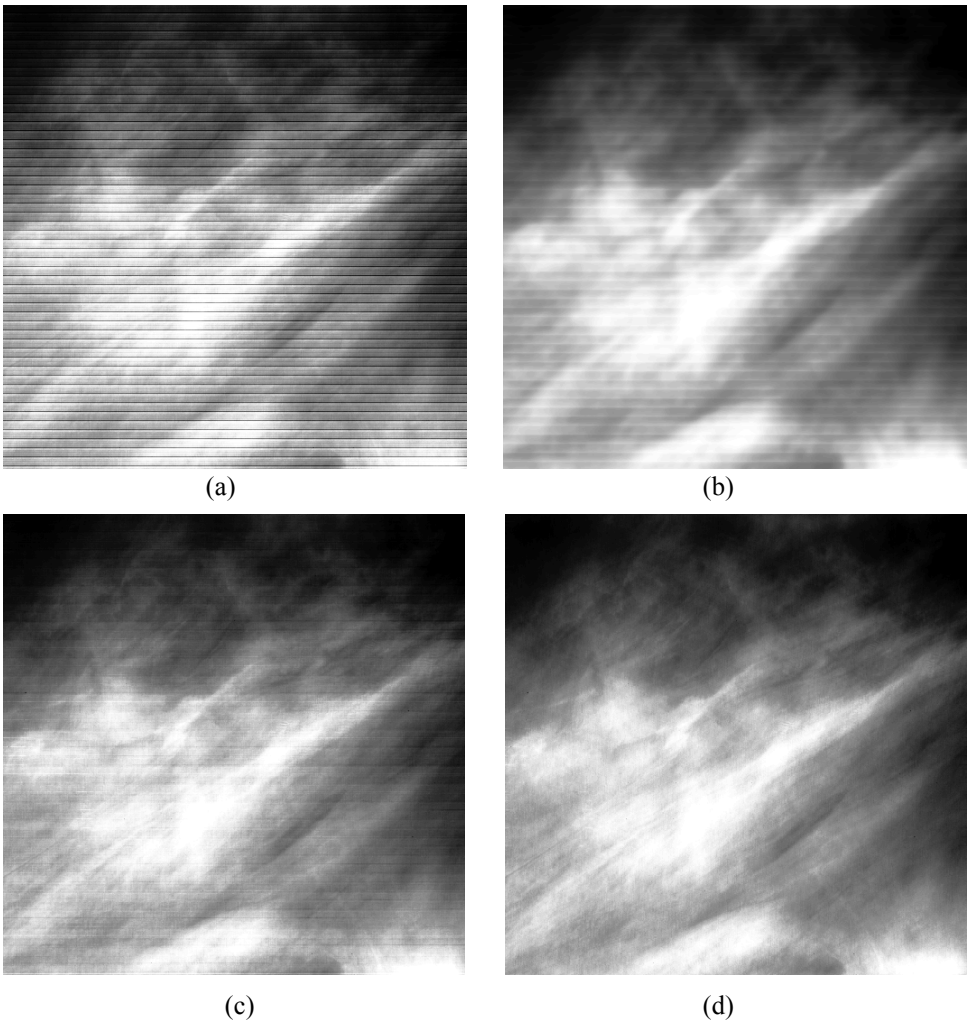

(a) (b)

(c) (d)

Figure 2. (a) Original image from MODIS Aqua band 27 (6.535-6.895µm) captured on November 10th 2009, western California. (b) Destriped image with a low-pass filter (c) Destriped image with histogramm matching (d) Destriped image with new technique.

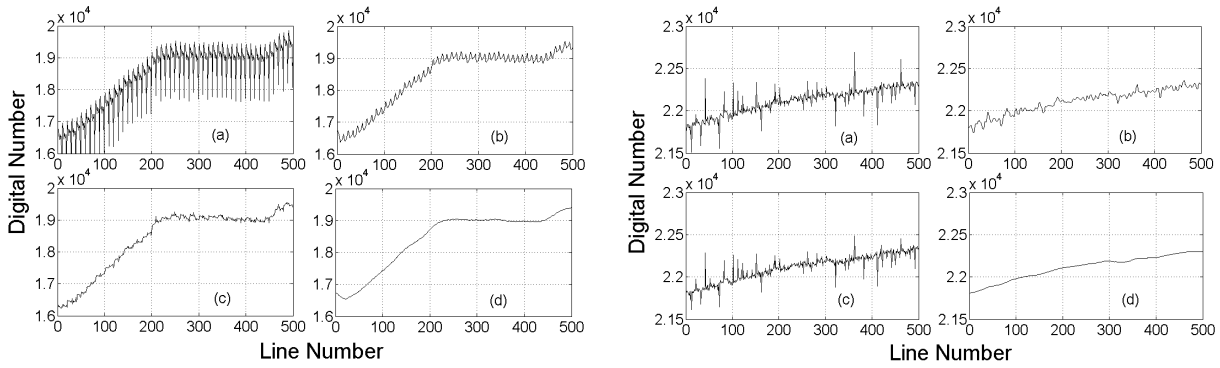

Figure 3. Mean cross-track profiles of figure 2 and 4 images (a) Original MODIS Aqua band 27 and Terra band 33 (b) Destriped image with low-pass filter (c) Destriped image with histogram matching (d) Destriped image with the new technique.

On the contrary, for all tested images, GBIDA provides a very smooth curve. Obviously, the analysis of cross-track profiles itself is not sufficient to assess the quality of destriping. Low-pass filtering also provides a good smoothing of cross-track profiles but at the cost of a significant loss of details from the original signal. Figure 5 represents the mean column power spectrum as a function of normalized frequency before and after destriping. To improve visibility, the spectral magnitudes are plotted with a logarithmic scale. Detector-to-detector stripes and mirror side banding translates in these graphs as clear pulses in the frequency domain. Histogram matching does reduce the pulses amplitude but it does not process random stripes. Although low-pass filtering can reduce all types of stripes, figures 5b indicate a significant bias in the resulting power spectrum. With the GBIDA approach, frequency components related to periodic stripes are extremely attenuated, and the power spectrums show no evidence of random stripes. To go further and provide a quantitative assessment of our destriping technique, we evaluate several qualitative indexes.

Noise Reduction Ratio and Image Distortion

Let us denote by P_0 (resp. Q_0) the ensemble averaged power spectrums down the columns (resp. lines) of the original image and by P_1 (resp. Q_1), the averaged power spectrums down the columns (resp. lines) of the destriped images. Assuming:

$$N_0 = \sum_{f=f_s} P_0(f) \qquad S_0 = \sum_{f} Q_0(f)$$
$$N_1 = \sum_{f=f_s} P_1(f) \qquad S_1 = \sum_{f} Q_1(f) \tag{14}$$

with **fs** the frequency related to stripes, noise reduction (NR) and image distortion (ID) are defined as:

$$NR = \frac{N_0}{N_1} \qquad ID = \frac{S_0}{S_1} \tag{15}$$

A similar image distortion index was used in (Chen et al. 2003), but its definition makes use of averaged power spectrums down the columns (instead of lines) and thus does not take into account the presence of noisy stripes. As a consequence, the histogram matching technique will provide illusive ID values equal to 1. Noise reduction and image distortion values results are reported in table 1.

Improvement Factors of Radiometric Quality

In (Corsini et al. 2000), two improvement factors IF have been defined and used. Let us evaluate the sequences:

$$d_R[j] = m_{I_R}[j] - m_I[j] \qquad d_E[j] = m_{I_E}[j] - m_I[j]$$
$$\Delta_{I_R}[j] = m_{I_R}[j] - m_{I_R}[j-1] \qquad \Delta_{I_E}[j] = m_{I_E}[j] - m_{I_E}[j-1] \tag{16}$$

where $\mathbf{m_{IR}[j]}$ (resp. $\mathbf{m_{IE}[j]}$) is the mean radiance value of the jth line in the raw image (resp. destriped image). $\mathbf{m_I[j]}$ is the mean value of the jth line in the image destriped with a low-pass filter. We recall the radiometric improvement factors definition:

$$IF1 = 10\log_{10}\frac{\sum_j d_R^2[j]}{\sum_j d_E^2[j]} \qquad IF2 = 10\log_{10}\frac{\sum_j \Delta_{I_R}^2[j]}{\sum_j \Delta_{I_E}^2[j]} \tag{17}$$

IF1 and IF2 values are reported in table 2.

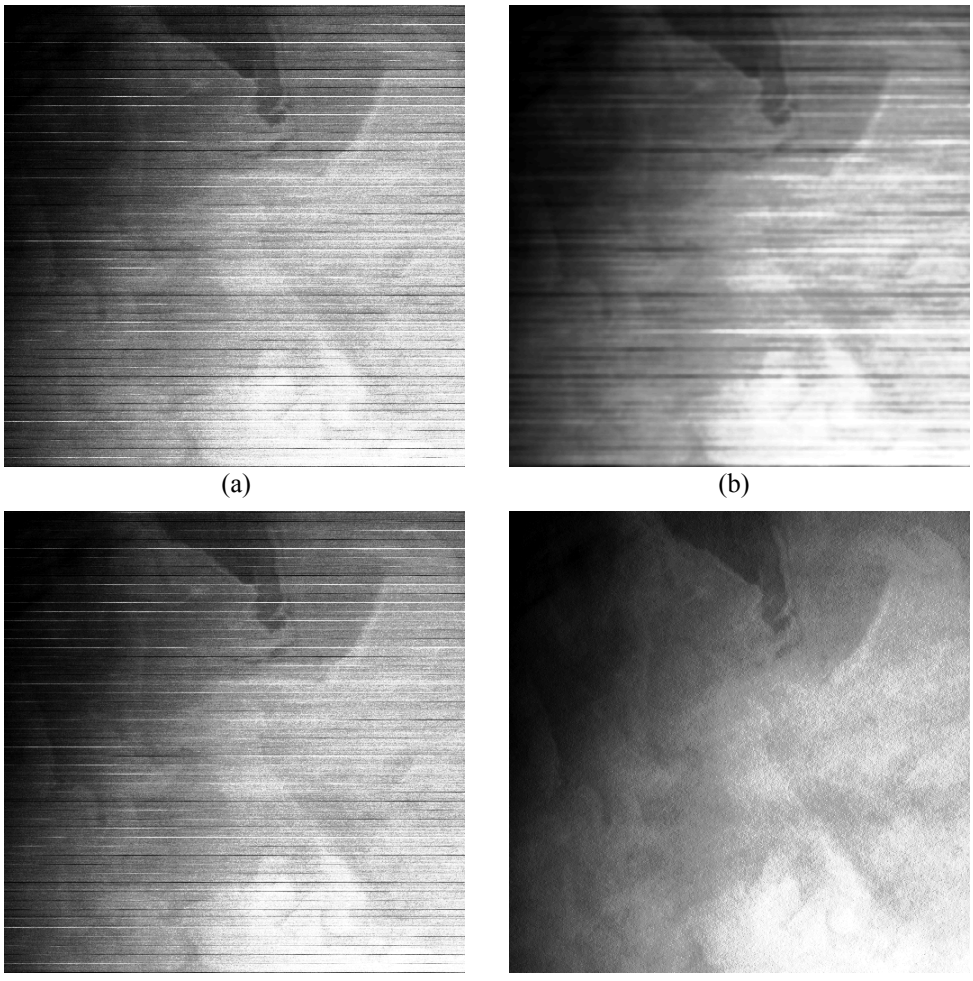

(a) (b) (c) (d)

Figure 4. (a) Original image from MODIS Terra band 33 (13.185-13.485 µm) captured on March 4, 2009, western California. (b) Destriped image with a low-pass filter (c) Destriped image with histogramm matching (d) Destriped image with new technique.

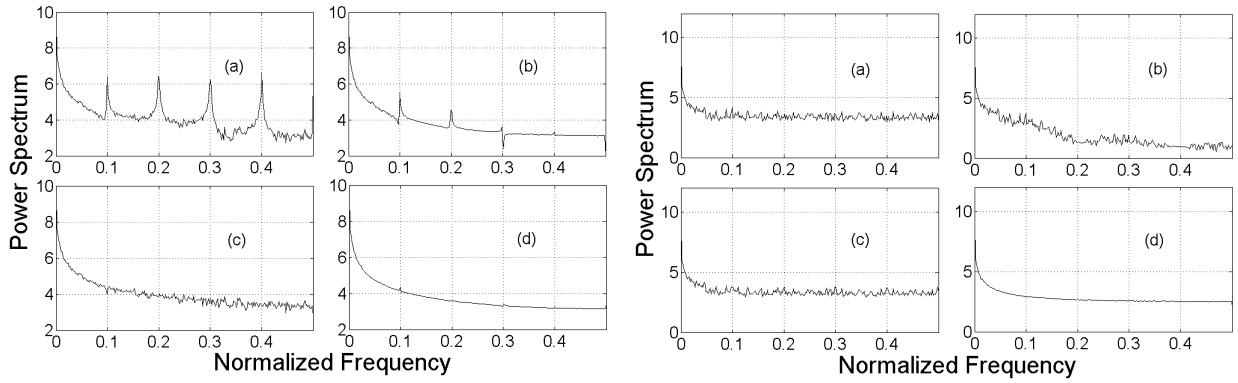

Figure 5. Mean column power spectrum of figure 1 and 2 images. (a) Original MODIS Aqua band 27 and Terra Band 33 (b) Destriped image with low-pass filter (c) Destriped image with histogram matching (d) Destriped image with the new technique.

Inverse Coefficient of Variance (ICV)

The inverse coefficient of variation is defined as:

$$ICV = \frac{R_m}{R_S} \tag{18}$$

where $\mathbf{R_m}$ and $\mathbf{R_s}$ are the mean and standard deviation of pixel values. The ICV index is computed in homogeneous regions within a window of 10×10 pixels. The results of ICV are reported in table 3.

CONCLUSION AND FUTUR WORK

In this paper, a new destriping algorithm is described and applied to MODIS images heavily affected by detector-to-detector stripes, mirror side stripes and random stripes. Aside the great qualitative improvement shown in cross-track profiles and columns power spectrums, quantitative measurements reported in tables 1 to 3 indicate very efficient and robust results. Unlike other methods, our technique increases noise reduction and radiometric improvement factors without distorting the image. The approach presented in this work relies on a variational framework that takes advantage of the striping effect unidirectional signature. It is shown that the destriped image can be estimated by minimizing an energy functional where the regularisation term is dependent on high order derivatives along the y-axis. Although not discussed in this paper, the implementation is easy and does not require a separation of images into detectors sub-images. One limitation that should be mentioned is the possible introduction of local blurring artifacts over very sharp edges (typically transitions between ocean, land and clouds). This is a well-known limitation of variational models based on quadratic energy functionals. Futur work will overcome this issue by focusing on edge-preserving variational models.

Table 1. Noise Reduction and Image distortion

BAND	INDEX	LOW-PASS	HISTOGRAM	PROPOSED
AQUA B27	NR	31.17	271.65	356.33
	ID	0.66	0.78	0.99
TERRA B33	NR	--	--	--
	ID	0.58	0.89	0.90

Table 2. Radiometric Improvement Factors

BAND	INDEX	HISTOGRAM	PROPOSED
AQUA B27	IF1	27.43	30.89
	IF2	50.85	85.44
TERRA B33	IF1	3.57	11.98
	IF2	4.1	84.01

Table 3. ICVS of the original and destriped images computed within a ten pixels by ten pixels window

BAND	AREA	ORIGINAL	LOW-PASS	HISTOGRAM	PROPOSED
AQUA B27	SAMPLE 1	56.16	96.76	61.82	93.69
	SAMPLE 2	46.39	171.05	173.76	204.19
TERRA B33	SAMPLE 1	245.07	947.36	264.96	584.46
	SAMPLE 2	305.79	1389	498.80	675.613

ACKNOWLEDGMENT

This research work has been conducted through funding from the Centre National d'Etudes Spatiales (CNES) and the French National Institute For Research in Computer Science and Control (INRIA). The author would like to thank Patrice Henry and Saïd Ladjal for their comments and suggestions for futur work.

REFERENCES

Algazi, V. R and G. E. Ford, 1981. Radiometric equalisation of nonperiodic striping in satellite data, *Comput.Graph. Image Process.*, 16(3):287-295

Antonelli, P., M. Di Bisceglie, R. Episcopo, and C. Galdi, 2004. Destriping MODIS data using IFOV overlapping, *Proc. IGARSS,* 7:4568-4571.

Chang, W. W., L. Guo, Z. Y. Fu, K. Liu, 2007. A new destriping method of imaging spectrometer images, *in Proc. ICWAPR,* 1:437-441

Chen, J. S., Y. Shao, H. D. Guo, W. Wang, and B. Zhu, 2003. Destriping CMODIS data by power filtering, *IEEE Trans. Geosci. Remote Sens.*, 41(9):2119-2124

Corsini, G., M. Diani, and T. Walzel, 2000. Striping removal in MOS-B data, *IEEE Trans. Geosci. Remote Sens.*, 38(3):1439-1446

Crippen, R. E., 1989. A simple spatial filtering routine, for the cosmetic removal of scan line noise from Landsat TM P-tape imagery, *Photogramm. Eng. Remote Sens.*, 55(3):327-331.

Di Bisceglie, M., R. Episcopo, C. Galdi, S. Liberata Ullo, 2009. Destriping MODIS data using overlapping field-of view method, *in IEEE Trans. Geosci. Remote Sens.*, 47(2):637-651.

Frankot, R.T., R. Chellappa, 1988. A method for enforcing integrability in shape from shading algorithms. *IEEE Trans. Pattern Anal. Mach. Intell,* 10:439–451,

Gumley, L., *Proc. MODIS Workshop*, 2002. URL: Western Autralian Satellite Technology and Applications Consortium

Horn, B. K. P. and R. J. Woodham, 1979. Destriping Landsat MSS images by histogram modification, *Comput. Graph. Image Process.*, 10:69-83.

Pan, J. J. and C. I. Chang, 1992. Destriping of Landsat MSS images by filtering techniques, *Photogramm. Eng. Remote Sens.*, 58(10):1417-1423.

Rakwatin, P., W. Takeushi, Y. Yasuoka, 2007. Stripe Noise Reduction in Modis data by combining histogram matching with facet filter, *IEEE Trans. Geosci. Remote Sens.*, 45(6):1844-1856.

Shen, H. and L. Zhang, 2009. A MAP-Based algorithm for destriping and inpainting of remotely sensed images, *in IEEE Trans. Geosci. Remote Sens.*, 47(5):1492-1502.

Simpson, J. J., and S. R. Yhann, 1994. Reduction of noise in AVHRR channel 3 data with minimum distortion, *IEEE Trans. Geosci. Remote Sens.*, 32(2):315-328.

Simpson, J. J., J. I. Gobat, and Frouin, R., 1995. Imporved destriping of GOES images using finite impulse response filters, *Remote Sens. Environ.*, 52(1):15-35.

Simpson, J. J., J. R. Stitt, and D. M. Leath, 1998. Improved finite impulse response filters for enhanced destriping of geostationary satellite data, *Remote Sens. Environ.*, 66(3):235-249.

Srinivasan, R., M. Cannon, and J. White, 1988. Lansat data destriping using power filtering, *Opt. Eng.*, 27(11):939-943.

Wegener, M., 1990. Destriping multiple detector imagery by improved histogram matching, *Int. J. Remote Sens.*, 11(5):859-875.